Materials Advances

ROYAL SOCIETY OF CHEMISTRY

PAPER

View Article Online
View Journal

Cite this: DOI: 10.1039/d6ma00084c

Ligand specific bioconjugation induced modulation of quantum yield in CdTe and graphene quantum dots

Akhil Khajuria,†[a] Jatinder Kaur,†[a] Hema K. Alajangi,†[b] Suraj Pratap Singh,[b] Pritiman Pothal,[a] Manpreet Singh,[a] Mahima Thakur,[a] Pavitra Ranawat,*[b] Ravi Pratap Barnwal *[b] and Gurpal Singh *[a]

Received 19th January 2026,
Accepted 29th April 2026

DOI: 10.1039/d6ma00084c

rsc.li/materials-advances

Quantum yield (QY) is essential for assessing the efficacy of fluorescent nanomaterials, especially for biosensing, bioimaging, and optoelectronic applications. It indicates the efficacy with which a material emits light when excited, and this efficacy directly influences our ability to detect and visualize biological activities at the molecular scale. The present study evaluated how bioconjugation of biologically relevant compounds to quantum dots (QDs) can influence their QY. We used cadmium telluride (CdTe) QDs capped with mercaptopropionic acid and nitrogen-doped graphene QDs (GQDs) as model systems. These were combined with folic acid, thiamine, cobalamin, bovine serum albumin, and DNA *via* EDC/NHS coupling chemistry. Our results indicated that QY is significantly influenced by the type of biomolecule and its concentration. While CdTe Qds exhibited superior intrinsic QY, GQDs displayed enhanced stability and biocompatibility, with certain conjugations significantly increasing their fluorescence. These findings underscore the significance of surface chemistry in modulating the optical properties of QDs. The present research thoroughly examines changes in QY during conjugation, providing essential insights for the development of advanced nanoprobes that are both fluorescent and stable, as well as biologically responsive. The research establishes a basis for developing modified, high-efficiency fluorescence systems for diagnostic, sensing, and therapeutic purposes.

1. Introduction

In the field of photochemistry, photophysics, and nanobiotechnology, the QY is a fundamental measure. Primarily in the form of fluorescence, this shows how effectively absorbed photons are converted into observable emission. QY provides an exact quantitative measurement of the brightness and performance of a luminous material.[1] The expression is the ratio of emitted photons to absorbed photons. A high QY ratio is absolutely necessary to guarantee sensitivity, reproducibility, and signal quality across several applications, including photovoltaics, optoelectronics, imaging, and sensing. QY directly governs the efficacy of photon-driven processes and serves as a benchmark for evaluating materials used in light-harvesting, emission-based sensing, and bioimaging.[1,2] In fluorescence-based biosensors, for instance, higher QY translates into more intense signals, improving detection limits and ensuring reliable performance in complex environments.[3] In live-cell imaging, high-QY fluorophores facilitate better resolution with lower excitation power, minimizing phototoxicity while preserving sample integrity.[4] In optical devices and LEDs, QY determines energy efficiency and stability. Thus, maximizing QY is essential for advancing both scientific exploration and commercial translation of luminescent nanomaterials.[5] While Otto Warburg applied these ideas to study photochemical efficiency in biological systems, early 20th century pioneers like Max Planck laid the groundwork for quantum theory. From this moment in time, the concept of the quantum yo–yo originates. QY has become a key performance measure in the evolution of photoluminescence (PL) based technology. With the development of QD, semiconductor nanocrystals defined by unique energy levels and size-tunable optical characteristics deriving from quantum confinement processes, the relevance of this subject has expanded dramatically.[1,6,7] QDs provide several notable benefits when compared to conventional fluorophores including broad absorption spectra, narrow emission bands, outstanding photostability, and notable Stokes shifts. QD's efficacy in practical uses is fundamentally related to their QY. Higher quantum yield not only boosts signal strength but also enhances spatial and temporal

[a] University Institute of Pharmaceutical Sciences, Panjab University, Chandigarh, India. E-mail: akhilkhajuria16@gmail.com, jatinderatwork92@gmail.com, pritimanpothal@gmail.com, manpreet296416@gmail.com, mahimathakur282000@gmail.com, gurpalsingh.ips@gmail.com
[b] Department of Biophysics, Panjab University, Chandigarh, India. E-mail: hemasai.biotech@gmail.com, surajonenonly@gmail.com, pavitraranawat@gmail.com, barnwal@pu.ac.in
† Akhil Khajuria, Jatinder Kaur and Hema K Alajangi are equal contributors.

resolution in real-time applications. Optimizing QY has thus become central to advancing various photonic tools, from clinical diagnostics to environmental sensors.[8,9] Furthermore, QY serves as a guiding parameter in the rational design of nanomaterials, helping researchers fine-tune structure function relationships for specific end uses. The photophysical characteristics of QDs, particularly their QY, are known to be profoundly influenced by surface chemistry. Biomolecular functionalization using proteins, peptides, aptamers, or nucleic acids has emerged as a promising strategy for potentially enhancing both the optical performance and biological compatibility of QDs.[10–12] By attaching biomolecules to the QD surface, it is anticipated that surface traps could be passivated, nonradiative decay minimized, and water solubility improved, all of which may contribute to significant increases in QY. Additionally, the functional groups present in biomolecules are expected to facilitate favorable electronic interactions at the QD interface, stabilizing excitons and potentially increasing radiative efficiency.[13,14] Importantly, the conjugation of biomolecules to QDs is hypothesized to offer dual benefits: not only improving QY but also enabling precise targeting in biological environments.[15] Such enhancements are especially relevant for applications in molecular diagnostics, cellular imaging, and biosensing, where both strong fluorescence and biological specificity are required.[16–18] Despite the well-recognized cytotoxicity associated with cadmium-based quantum dots, CdTe QDs were intentionally selected in this study as a model high quantum yield system for fundamental photophysical investigations rather than for translational or clinical applications. Their exceptionally bright emission and well-characterized surface chemistry make CdTe QDs a widely accepted reference platform for systematically examining how surface bioconjugation influences quantum yield. Importantly, all applications discussed in this work are strictly limited to *in vitro* diagnostic and analytical sensing contexts, where the nanomaterials are not administered to living organisms. Under such controlled conditions, CdTe QDs remain a commonly used and effective tool for high-sensitivity fluorescence studies. In parallel, graphene quantum dots (GQDs) were included as a representative carbon-based nanomaterial to address biocompatibility-related concerns and to provide a comparative framework. This dual-material approach enables direct evaluation of how different core compositions respond to identical bioconjugation strategies, while highlighting GQDs as a potential low-toxicity alternative for future diagnostic translation.

In this work, we aim to systematically investigate how the QY of CdTe QDs and GQDs is affected by conjugation with DNA aptamers, peptides, and proteins. CdTe quantum dots and graphene quantum dots were selected as representative materials to explore this modulation in QY.

2. Material and methods

2.1. Methods

2.1.1. Synthesis and characterization of CdTe QDs and GQDs. The synthesis and characterization of the QDs have been described in the SI.

2.1.2. Bioconjugation of QDs with folic acid (FA)/bovine serum albumin (BSA)/thiamine/cobalamin/DNA/cholesterol and cholecalciferol. To facilitate ligand specific bioconjugation, CdTe QDs and GQDs, each prepared at a concentration of 1 mg mL^{-1}, were first activated using carbodiimide chemistry. Specifically, 25 μL of *N*′ ethyl carbodiimide hydrochloride (EDC; 400 mM in methanol) and 25 μL of *N* hydroxysuccinimide (NHS; 100 mM in methanol) were added under constant stirring at room temperature (RT) and incubated for 30 minutes. Following activation, the CdTe MPA QDs and GQDs were incubated with varying concentrations (1 μM, 2 μM, 5 μM, 25 μM, 50 μM, and 100 μM) of selected ligands including FA, BSA, thiamine, cobalamin, DNA, cholesterol, and cholecalciferol, prepared in phosphate buffered saline (PBS; pH 7.4).

To ensure uniformity and reproducibility of conjugation across all ligand systems, the bioconjugation process was performed under strictly controlled conditions. The reaction mixtures were kept in dark conditions to protect the EDC/NHS activated intermediates from light-induced decomposition, maintained at a temperature of 0–4 °C, and continuously stirred (30 minutes) to facilitate homogeneous interaction between the activated quantum dots and ligands. The reactions were conducted in phosphate buffer (pH 7.4) to maintain physiological conditions, ensuring stability of both the nanoparticle surface and the biomolecules throughout the coupling process. These controlled parameters were found to yield reproducible conjugation efficiency and stable fluorescent properties in all bioconjugated samples.[19] Post conjugation, the QDs were purified by centrifugation at 14 000 rpm for 15 minutes to remove unbound ligands. This washing step was repeated three times to ensure complete removal of excess free FA, BSA, thiamine, cobalamin, DNA, cholesterol, and cholecalciferol. All other experimental conditions were maintained consistently across samples.

2.1.3. Measurement of QY

The fluorescence QY (Φ_F) was determined using the comparative method. Here, the Φ_F of a sample was calculated by comparing the fluorescence intensity of unconjugated and conjugated CdTe-MPA QDs and GQDs to the reference sample Φ_F (rhodamine 6G) using eqn (1). Therefore, the fluorescence QY of the unknown is obtained from the product of the QY of the reference.[20]

$$Q_S = Q_R\,(A_R/A_S)\,(E_S/E_R)\,(\eta_S/\eta_R)^2 \quad (1)$$

Q = fluorescence QY, η = refractive index of the solvent, A = absorbance of the solution, E = integrated fluorescence intensity of the emitted light, Subscripts 'R' and 'S' refer to the reference and unknown fluorophore respectively.

3. Results and discussion

3.1. Synthesis and Characterization of CdTe-MPA QDs and GQDs

3.1.1. Synthesis of QDs. CdTe QDs (Fig. 1A) and GQDs (Fig. 1C) were synthesized as discussed in the methods sections of SI, owing to the distinct advantages offered by these methods, as enumerated in the SI.

Fig. 1 Photographic image of QDs. (A) CdTe-MPA QDs showing different emission colors during synthesis (I and II) 15 min, (green); (III and IV) 30 min, (green-yellow); (V, VI and VII) 45 min, (yellow); (VIII) 60 min, (yellow-orange); (IX) 75 min (orange-red); (X) 90 min, 120 min (red). (B) GQDs after synthesis under visible light. (C) GQDs showing blue emission colour under UV light.

3.1.2. Bioconjugation of QDs with folic acid (FA)/BSA/thiamine (vitamin B_1)/cobalamin (vitamin B_{12})/DNA/cholecalciferol/cholesterol. The conjugation of cadmium telluride mercaptopropionic acid quantum dots (CdTe–MPA QDs) and graphene quantum dots (GQDs) with various biomolecules was achieved using 1-ethyl-3-(3-dimethylaminopropyl) carbodiimide (EDC) and *N*-hydroxysuccinimide (NHS) chemistry. Initially, the quantum dots were activated using EDC/NHS, generating a reactive NHS ester intermediate. Upon reaction with biomolecules containing primary amine groups, an amide bond was formed, leading to the successful attachment of the biomolecule to the QD surface. EDC, a zero-length crosslinker, was utilized due to its widespread use and efficiency in producing stable conjugates under controlled conditions with high yields.[21–23]

3.1.3. Fluorescence spectroscopy. Fluorescence properties of the synthesized QDs were evaluated using a spectrofluorometer. CdTe-MPA QDs exhibited a strong emission peak centered at 630 nm upon excitation at 390 nm, consistent with size-dependent optical behavior commonly reported for CdTe nanocrystals and corresponding to their orange-red fluorescence. This observation is supported by the particle size characterization provided in the SI, which confirms the nanoscale dimensions of the CdTe-MPA QDs, rather than relying on PL data alone to infer quantum confinement effects. In contrast, GQDs displayed excitation-dependent emission behavior, with maximum excitation and emission observed at 335 nm and 423 nm, respectively. The emission spectra of both types of QDs were narrow and symmetrical, indicating good spectral resolution and signal clarity. These optical characteristics suggest that CdTe QDs and GQDs are suitable candidates for use as fluorescent probes in analytical and biomedical applications (Fig. 2).[24,25]

3.1.4. Effect of concentration on emission intensity. As illustrated in Fig. 3a, hydrophilic CdTe-MPA QDs exhibit a strong and well-defined emission peak centered at approximately 614 nm when excited in the 380–400 nm wavelength range. A progressive reduction in quantum dot concentration leads to a corresponding decrease in photoluminescence (PL) intensity, indicating a direct and systematic relationship between concentration and emission output. A slight shift in the emission wavelength is also observed at different concentrations, which can be attributed to excitation-related effects and variations in surface electronic states rather than changes in particle size, consistent with reported behavior for semiconductor quantum dots. Similarly, Fig. 3b presents the emission characteristics of graphene quantum dots (GQDs), showing a prominent emission peak at 422 nm under excitation at 335 nm. An increase in GQD concentration results in a proportional enhancement of fluorescence intensity, reflecting the additive contribution of emissive centers within the system. This concentration-dependent fluorescence response highlights the stable and predictable optical behavior of GQDs. Overall, the observed trends for both CdTe-MPA QDs and GQDs confirm that fluorescence intensity scales directly with quantum dot concentration while maintaining consistent emission characteristics.

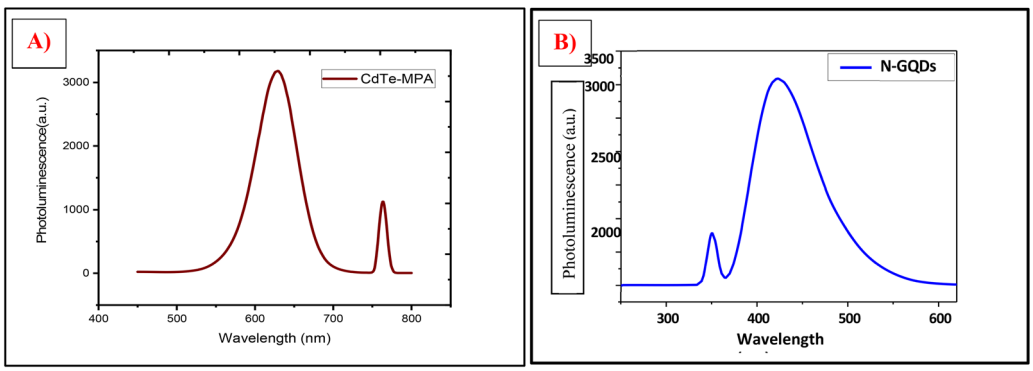

Fig. 2 PL spectra of (A) CdTe-MPA QDs and (B) GQDs.

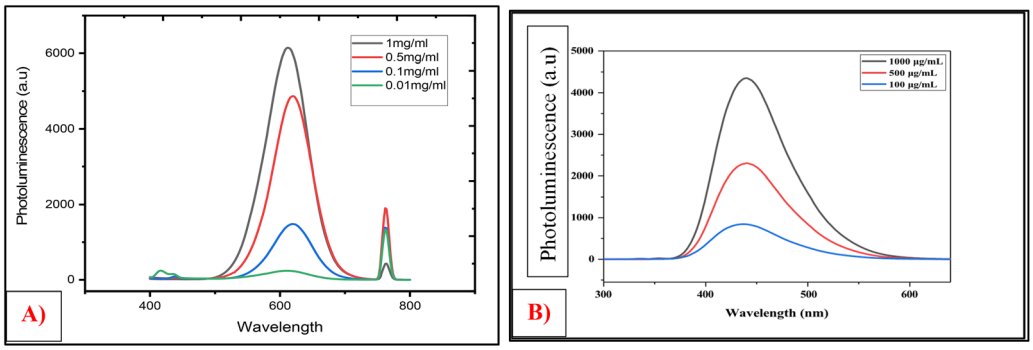

Fig. 3 Effect of concentration on PL of (A) CdTe-MPA QDs and (B) GQDs.

3.1.5. Fluorescence spectroscopy of conjugated QDs. The emission spectra of nonconjugated and ligand-conjugated QDs, illustrated in Fig. 4, showcase distinct PL features that vary based on the specific ligands and their concentrations. Fig. 4A(i) illustrates that as the concentration of FA conjugated CdTe-MPA QDs increases from 1 μM to 50 μM, a gradual decrease in emission intensity is observed, along with a slight shift of the emission peak toward longer wavelengths. This behavior is attributed to surface modifications introduced during the FA bioconjugation process. The attachment of FA molecules alters the surface electronic environment of the quantum dots, leading to the formation or modulation of surface trap states and enhanced nonradiative recombination pathways, which collectively result in partial fluorescence quenching. The minor redshift in emission is therefore associated with excitation-related effects and surface-state interactions rather than changes in the intrinsic band-edge energy levels or core structure of the CdTe quantum dots. Such surface functionalization-induced photoluminescence changes have been widely reported for CdTe-based quantum dots and are consistent with established literature on ligand-QD interactions. Conversely, Fig. 4A(ii) illustrates that FA-conjugated GQDs exhibited a rise in fluorescence intensity that was influenced by concentration, likely resulting from the interactions between FA and NH sites in nitrogen-doped GQDs.[26–28] In Fig. 4A(iii), we can see that as the concentration of BSA increased, the emission intensity of the BSA-conjugated CdTe MPA QDs decreased, accompanied by a slight redshift.[29,30] On the other hand, Fig. 4A(iv) shows that GQDs exhibited a different pattern, where the conjugation with BSA resulted in a rise in PL intensity. This increase is associated with the formation of amide bonds that contribute to stabilizing the surface.[31,32] Furthermore, Fig. 4A(v) illustrates that when thiamine is linked to CdTe MPA QDs, there is a marked reduction in intensity from 1 μM to 50 μM, with the most significant shift happening between 1 μM and 5 μM. Fig. 4A(vi) illustrates a comparable pattern of quenching that depends on concentration in thiamine-conjugated GQDs. This indicates that a shared mechanism is likely responsible for the reduction of photoluminescence due to surface interactions. Fig. 4B(i) and (ii) illustrate that as the concentration of cobalamin-conjugated CdTe MPA QDs and GQDs increased to 100 μM, there was a noticeable decrease in emission intensities and slight redshifts. This suggests that the bioconjugation process led to alterations in the surface electronic properties. Following this trend, Fig. 4B(iii) and (iv) illustrate that DNA-conjugated CdTe MPA QDs and GQDs showed a consistent decline in fluorescence intensity as the concentration increased from 1 μM to 10 μM. This indicates that when DNA binds to the QDs, it changes their surface, which in turn affects how they emit light.[33] In contrast to these ligands, Fig. 4B(v) and (vi) indicate that mixing cholesterol and vitamin D3 with CdTe MPA QDs did not result in any significant changes in the emission spectra across various dosages, implying minimal to no interaction. In a similar vein, Fig. 4B(vii) and (viii) for GQDs displayed intricate yet somewhat unclear spectral characteristics. It appears that the quenching we see is likely caused by protonated groups attracting photoexcited electrons, rather than a direct interaction between the ligands and the quantum dots. The results indicate that the optical characteristics of both CdTe MPA QDs and GQDs are significantly affected by the kind and amount of bioconjugated ligands used. When there are groups that donate electrons or interact on the surface, it alters the electronic transitions, which then influences the fluorescence output. This holds significant promise for how they could be used in biosensing and diagnostic tools.

3.1.6. Fourier-transform infrared spectroscopy (FTIR). FTIR spectroscopy was utilized to verify the surface functionalization of CdTe-MPA QDs and GQDs with diverse biomolecules, including FA, BSA, thiamine, cobalamin, DNA, cholesterol, and cholecalciferol. In the FA-conjugated CdTe QDs (Fig. 5A), a notable shift in the carbonyl stretching vibration from 1561.37 cm^{-1} in non-conjugated QDs to 1640.54 cm^{-1} was found, signifying the establishment of an amide bond (–CONH).[34,35] Likewise, GQDs conjugated with FA (Fig. 5B) exhibited extensive N–H and O–H stretching bands about 3440 cm^{-1}, in addition to C–N vibrations within the range of 1100–1400 cm^{-1},[36,37] thereby affirming effective conjugation.[38] The conjugation of BSA was demonstrated by the emergence of amide I and II bands within the range of 1639.4–1654.32 cm^{-1} for CdTe QDs[39–41] (Fig. 5C) and approximately 1640 cm^{-1} for GQDs (Fig. 5D), in addition to C–N stretching at around 1400 cm^{-1}.[42] Thiamine-conjugated CdTe QDs demonstrated a shift in the –C═O band to 1640.12 cm^{-1} (Fig. 5E),[43–45] whereas thiamine-GQDs (Fig. 5F) exhibited broad N–H and O–H stretching about 3400 cm^{-1} and C–H

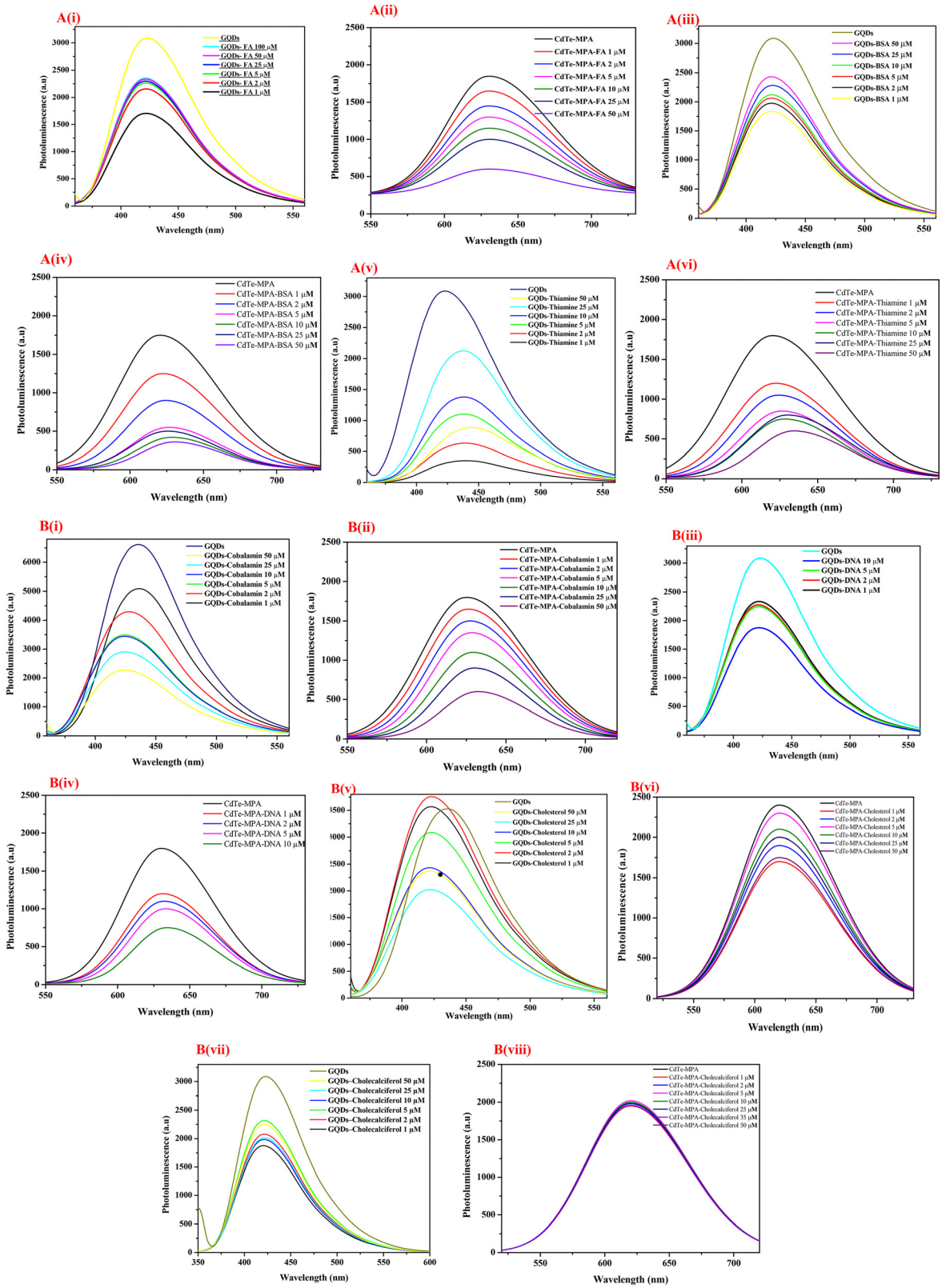

Fig. 4 PL spectra of non-conjugated and ligand-conjugated QDs, including CdTe-MPA QDs and GQDs, under various ligand concentrations. The ligands used for bioconjugation include FA (Fig. 4A(i) and (ii)), BSA (Fig. 4A(iii) and (iv)), thiamine (Fig. 4A(v) and (vi)), cobalamin (Fig. 4B(i) and (ii)), and DNA (Fig. 4B(iii) and (iv)), along with cholesterol and cholecalciferol (Fig. 4B(v), (vi), (vii), and (viii)). The spectral responses exhibit ligand-specific variations in emission intensity and bathochromic shifts upon excitation, highlighting the surface interaction and bioconjugation behavior of both QD types.

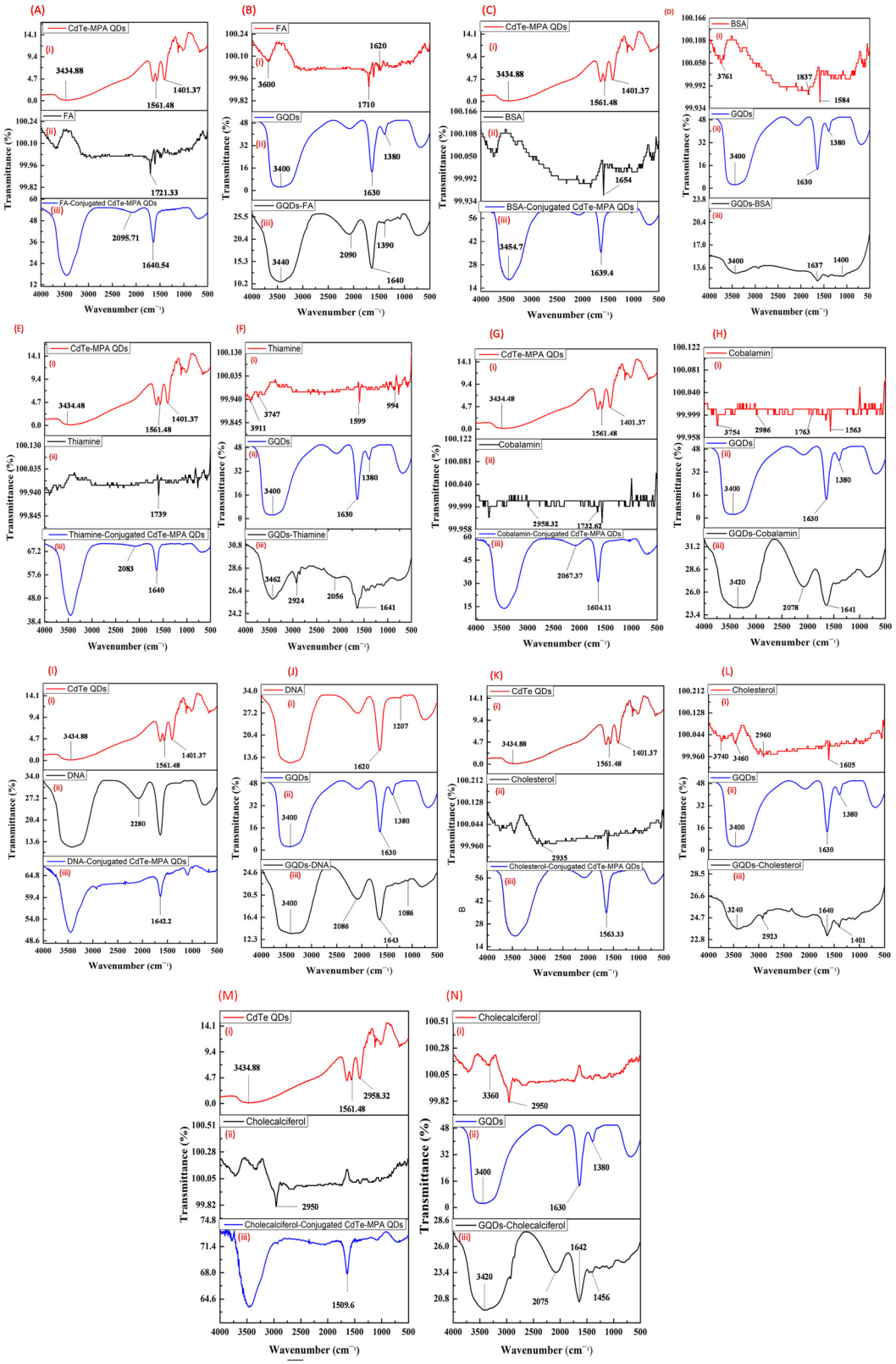

Fig. 5 FTIR spectra showing the surface functionalization and bioconjugation of QDs, including CdTe-MPA QDs and GQDs, with various biological ligands. Subfigures illustrate FTIR spectra of (A) (i) CdTe-MPA QDs, (ii) FA, and (iii) FA-conjugated CdTe-MPA QDs; (B) (i) GQDs, (ii) FA, and (iii) FA-conjugated GQDs; (C) (i) CdTe-MPA QDs, (ii) BSA, and (iii) BSA-conjugated CdTe-MPA QDs; (D) (i) BSA, (ii) GQDs, and (iii) BSA-conjugated GQDs; (E) (i) CdTe-MPA QDs, (ii) thiamine, and (iii) thiamine-conjugated CdTe-MPA QDs; (F) (i) thiamine, (ii) GQDs, and (iii) thiamine-conjugated GQDs; (G) (i) CdTe-MPA QDs, (ii) cobalamin, and (iii) cobalamin-conjugated CdTe-MPA QDs; (H) (i) cobalamin, (ii) GQDs, and (iii) cobalamin-conjugated GQDs; (I) (i) CdTe-MPA QDs, (ii) DNA, and (iii) DNA-conjugated CdTe-MPA QDs; (J) (i) DNA, (ii) GQDs, and (iii) DNA-conjugated GQDs. Negative control FTIR spectra of non-binding ligands: (K) (i) CdTe-MPA QDs, (ii) cholesterol, and (iii) cholesterol-mixed CdTe-MPA QDs; (L) (i) GQDs, (ii) cholesterol, and (iii) cholesterol-mixed GQDs; (M) (i) CdTe-MPA QDs, (ii) cholecalciferol, and (iii) cholecalciferol-mixed CdTe-MPA QDs; (N) (i) GQDs, (ii) cholecalciferol, and (iii) cholecalciferol-mixed GQDs.

stretching at approximately 2924 cm^{-1}, signifying effective coupling. The FTIR spectra of conjugated CdTe QDs for cobalamin exhibited a carbonyl peak shift to 1604.11 cm^{-1} (Fig. 5G), while GQDs demonstrated wide absorption in the 3200–3500 cm^{-1} region, indicative of O–H and N–H groups (Fig. 5H). DNA-functionalized CdTe QDs demonstrated a –C═O shift to 1642.2 cm^{-1} (Fig. 5I), while DNA-GQDs (Fig. 5J) revealed novel peaks at 2086 and 1643 cm^{-1}, in addition to a broad O–H/N–H stretch near 3400 cm^{-1}, suggesting potential hydrogen bonding or covalent connections.[39,43–45] The FTIR spectra of cholesterol and cholecalciferol exhibited neither carboxylic acid (–COOH) or amide (–CONH) bands, indicating an absence of covalent attachment to CdTe QDs (Fig. 5K and L). In GQDs containing cholesterol (Fig. 5M), peaks at 3740 and 3460 cm^{-1} (O–H) and 2923–2960 cm^{-1} (C–H) signified non-covalent interactions. Graphene quantum dots (GQDs) combined with cholecalciferol (Fig. 5N) exhibited peaks at 2075 cm^{-1} (C≡C), 1456 cm^{-1} (C–H bending), and a pronounced C═C alkene stretch at 1642 cm^{-1}, indicating successful interaction under optimum conditions.[46] The FTIR analyses together validated the selective and effective functionalization of QDs and GQDs with several physiologically pertinent ligands, facilitating their prospective application in targeted delivery and bioimaging.

4. Proposed mechanism of QY modulation

The modulation in QY following ligand conjugation arises from the combined effects of surface passivation and ligand-induced electronic interactions. Ligands possessing electron-donating functional groups (–NH_2, –COOH) effectively reduce non-radiative surface trap states, leading to enhanced photoluminescence. In contrast, bulky or highly charged ligands (*e.g.*, DNA, thiamine) can introduce localized dipolar electric fields or π–π stacking interactions that perturb excitonic recombination, resulting in partial fluorescence quenching. Supporting evidence from FTIR and PL spectra (Fig. 4 and 5) confirms the successful covalent attachment of biomolecules and the corresponding shifts in emission behavior. The FTIR results demonstrate characteristic amide bond formation, verifying ligand coupling to the QD surface, while PL spectral red shifts indicate slight modifications in surface potential and electronic density near the band edge. These observations collectively support that ligand conjugation modulates QY primarily through trap passivation and electronic coupling effects, establishing a mechanistic link between surface chemistry and photophysical performance.[47–50]

5. Measurement of QY

Mean PL QYs of the CdTe-MPA QDs, N-GQDs and conjugated QDs were measured using rhodamine 6G.

5.1. Control experiments and ligand specificity of QY modulation

To confirm that the observed quantum yield (QY) modulation was specific to covalent bioconjugation, control experiments were conducted using both unmodified and non-reactive quantum dots (QDs). Unconjugated CdTe-MPA QDs and GQDs were used as baseline controls and showed consistent emission intensity and QY under identical experimental conditions. In contrast, bioconjugation with ligands containing amine groups such as folic acid, BSA, thiamine, cobalamin, and DNA which produced distinct variations in QY, confirming the occurrence of covalent coupling through EDC/NHS-mediated amide bond formation. Non-reactive ligands, including cholesterol and cholecalciferol, which lack primary amine functionality, were employed as negative controls and exhibited negligible changes in fluorescence intensity or QY. FTIR spectra further supported this observation by showing characteristic amide I and II bands only in amine-bearing conjugates, while control samples displayed no such features. These results collectively confirm that QY modulation occurred exclusively in ligand systems capable of covalent conjugation and not due to nonspecific adsorption or environmental effects, validating the ligand-specific nature of the observed optical behavior.[51–54]

5.2. Measurement of QY of FA-conjugated QDs

Table 1 displays the QY of nonconjugated and FA-conjugated QDs. The plot of QY at various concentrations is shown in Fig. 6A and B. Therefore, as shown by the results, the QY of conjugated QDs (CdTe-MPA-FA 50 μM) over non-conjugated one was about 51.2%. Since QY is a measurement of fluorophore optical quality, the resulting values of QY suggested that the QDs fluorescent properties had been substantially retained even after conjugation with folic acid.[55] Therefore, as shown by the results, the QY of conjugated GQDs (GQDs-FA 50 μM) over non-conjugated ones was about 54.4%. This value indicates that the fluorescence efficiency of these conjugated GQDs remains relatively high compared to non-conjugated GQDs, indicating that the conjugation process not only preserves but

Table 1 QY of nonconjugated and FA-conjugated QDs

S. no	Sample	Relative quantum yield (%)	SEM	Sample	Relative quantum yield (%)	SEM
1.	CdTe-MPA	100%	2.19	GQDs	100%	3.06
2.	CdTe-MPA-FA 1 μM	91.7%	2.77	GQDs-FA 1 μM	91.7%	2.27
3.	CdTe-MPA-FA 2 μM	83.3%	2.52	GQDS-FA 2 μM	83.3%	2.79
4.	CdTe-MPA-FA 5 μM	72.6%	2.06	GQDs-FA 5 μM	75%	3.62
5.	CdTe-MPA-FA 10 μM	64.3%	2.49	GQDs-FA 5 μM	66.7%	3.09
6.	CdTe-MPA-FA 25 μM	57.1%	2.37	GQDs-FA 25 μM	60%	3.55
7.	CdTe-MPA-FA 50 μM	51.2%	2.68	GQDs-FA 50 μM	54.4%	2.2

Table 2 QY of nonconjugated and BSA-conjugated QDs

S. no	Sample	Relative quantum yield (%)	SEM	Sample	Relative quantum yield (%)	SEM
1.	CdTe-MPA QDs	100%	3.07	N-GQDs	100%	3.73
2.	CdTe-MPA-BSA 1 μM	95.2%	2.4	GQDs-BSA 1 μM	95.6%	3.74
3.	CdTe-MPA-BSA 2 μM	89.3%	2.2	GQDs-BSA 2 μM	91.7%	2.63
4.	CdTe-MPA-BSA 5 μM	82.1%	2.33	GQDs-BSA 5 μM	84.4%	3.69
5.	CdTe-MPA-BSA 10 μM	75%	2.15	GQDs-BSA 10 μM	76.7%	2.55
6.	CdTe-MPA-BSA 25 μM	67.9%	3.16	GQDs-BSA 25 μM	69.4%	3.37
7.	CdTe-MPA-BSA 50 μM	61.9%	3.15	GQDs-BSA 50 μM	63.9%	3.06

also potentially enhances the fluorescence characteristics of the GQDs.

5.3. Measurement of QY of BSA-conjugated QDs

Table 2 displays the QY of BSA-conjugated and nonconjugated QDs. The plot of QY at various concentrations is shown in Fig. 7. The results indicate that, when compared to non-conjugated QDs, the QY of conjugated QDs (CdTe-MPA-BSA 50 μM) was approximately found to be 61.9%. QY values showed that the QDs' fluorescent characteristics had thus largely survived conjugation.[55] The results indicate that, when compared to non-conjugated GQDs, the QY of conjugated GQDs (N-GQDs-BSA 50 μM) was found to be 63.9%. This value indicates that the fluorescence efficiency of these conjugated GQDs remains relatively high compared to non-conjugated GQDs indicating that the conjugation process not only preserves but also potentially enhances the fluorescence characteristics of the GQDs.

5.4. Measurement of QY thiamine-conjugated QDs

The QY of nonconjugated and thiamine-conjugated QDs is shown in Table 3. Fig. 8 displays the plot of QY at various concentrations. The QY of conjugated QDs (CdTe-MPA-thiamine QDs 50 μM) compared to non-conjugated ones was found to be 58.3%. Therefore, the fluorescent properties of the QDs had thus been largely preserved even after conjugation, as shown by QY values.[56] The QY of conjugated GQDs (GQDs-thiamine GQDs 50 μM) compared to GQDs ones was found to be 58.3%. The findings indicate that the thiamine and GQDs mixture suggests that negatively charged GQDs electrostatically interact with the positively charged quaternary nitrogen in thiamine's thiazole ring. This interaction starts destabilizing and aggregating the GQDs with increased concentrations.[57] This lower QY indicates that, at certain concentrations, thiamine may significantly affect the fluorescent properties of the GQDs.

5.5. Measurement of QY cobalamin-conjugated QDs

The QY of nonconjugated and cobalamin-conjugated QDs is shown in Table 4. Fig. 9 displays the plot of QY at various concentrations. The QY of conjugated QDs (CdTe-MPA-cobalamin QDs 50 μM) compared to non-conjugated one was found to be 66.7%. Therefore, as shown by the results fluorescent properties of the QDs had been largely preserved even after conjugation with cobalamin.[56] The QY of conjugated GQDs (GQDs-cobalamin 50 μM) compared to

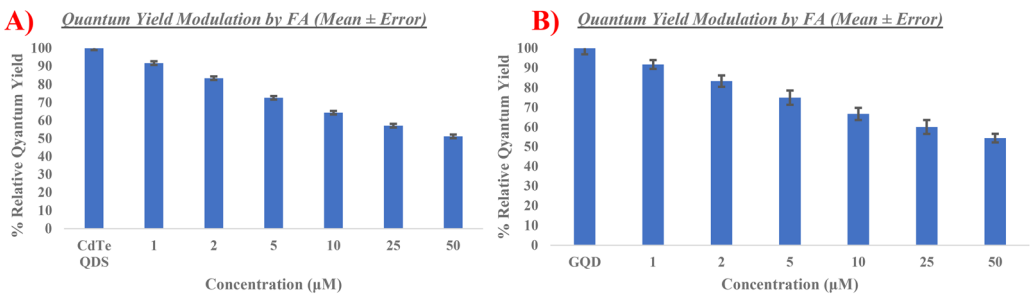

Fig. 6 (A) Plot of QY of CdTe-MPA QDs and CdTe-MPA-FA QDs at different concentrations (B) plot of QY of GQDs and GQDs-FA QDs at different concentrations.

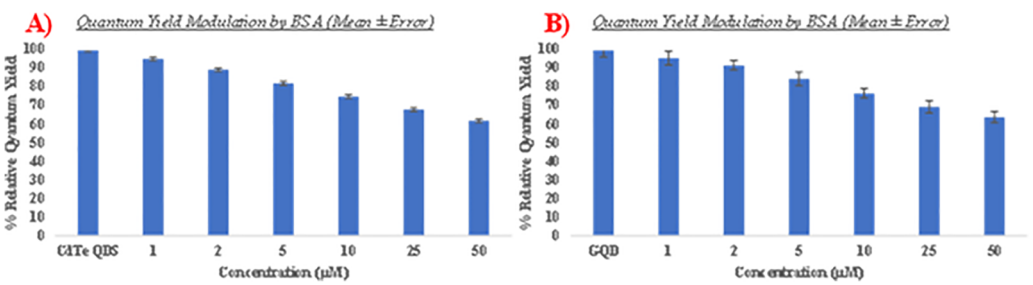

Fig. 7 (A) Plot of QY of CdTe-MPA and CdTe-MPA-BSA at different concentrations (B) plot of QY of GQDs and GQDs-BSA at different concentrations.

Table 3 QY of nonconjugated and thiamine-conjugated QDs

S. no	Sample	Relative quantum yield (%)		Sample	Relative quantum yield (%)	SEM
1.	CdTe-MPA QDs	100	2.51	GQDs	100%	4.01
2.	CdTe-MPA-thiamine 1 μM	92.9%	2.09	GQDs-thiamine 1 μM	93.3%	2.64
3.	CdTe-MPA-thiamine 2 μM	85.7%	2.18	GQDs-thiamine 2 μM	86.1%	4.07
4.	CdTe-MPA-thiamine 5 μM	78.6%	2.79	GQDs-thiamine 5 μM	78.9%	3.84
5.	CdTe-MPA-thiamine 10 μM	71.4%	2.76	GQDs-thiamine 10 μM	71.1%	2.5
6.	CdTe-MPA-thiamine 25 μM	64.3%	2.31	GQDs-thiamine 25 μM	63.9%	3.64
7.	CdTe-MPA-thiamine 50 μM	58.3%	2.7	GQDs-thiamine 50 μM	58.3%	3.01

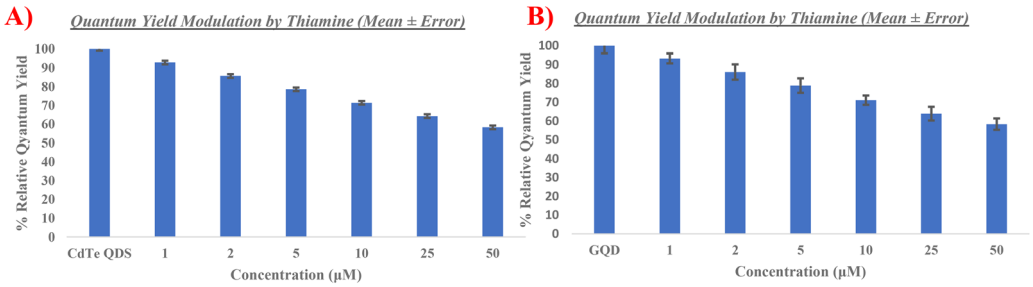

Fig. 8 (A) Plot of QY of CdTe-MPA and CdTe-MPA thiamine at different concentrations (B) plot of QY of GQDs and GQDs-BSA at different concentrations.

Table 4 QY of nonconjugated and cobalamin-conjugated QDs

S. no.	Sample	Relative quantum yield (%)	SEM	Sample	Relative quantum yield (%) (%)	SEM
1.	CdTe-MPA QDs	100%	2.52	N-GQDs	100%	3.07
2.	CdTe-MPA-cobalamin QDs 1 μM	96.4%	2.06	GQDs-cobalamin QDs 1 μM	97.2%	2.53
3.	CdTe-MPA-cobalamin QDs 2 μM	92.9%	3.06	GQDs-cobalamin QDs 2 μM	93.3%	3.58
4.	CdTe-MPA-cobalamin QDs 5 μM	86.9%	2.25	GQDs-cobalamin QDs 5 μM	87.8%	3.93
5.	CdTe-MPA-cobalamin QDs 10 μM	79.8%	3.12	GQDs-cobalamin QDs 10 μM	80.6%	2.67
6.	CdTe-MPA-cobalamin QDs 25 μM	72.6%	2.19	GQDs-cobalamin QDs 25 μM	73.3%	4.07
7.	CdTe-MPA-cobalamin QDs 50 μM	66.7%	2.97	GQDs-cobalamin QDs 50 μM	66.7%	3.46

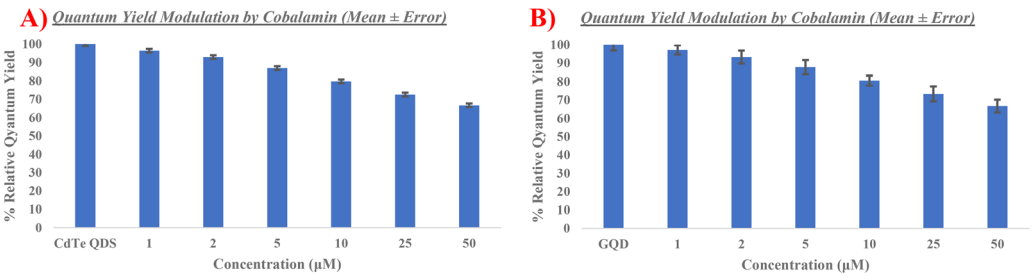

Fig. 9 (A) Plot of QY of CdTe-MPA QDs and CdTe-MPA-cobalamin QDs at different concentrations. (B) Plot of QY of GQDs and GQDs-cobalamin at different concentrations.

non-conjugated ones was found to be 66.7%. Therefore, the fluorescence characteristics of the GQDs remained stable despite conjugation with cobalamin.

5.6. Measurement of QY of DNA-conjugated QDs

The QY of nonconjugated and DNA-conjugated QDs is shown in Table 5. Fig. 10 displays the plot of QY at various concentrations. The QY of conjugated QDs (CdTe-MPA-DNA QDs 50 μM) compared to non-conjugated ones was found to be 58.3%. Therefore, the fluorescent properties of the QDs had thus been largely preserved even after conjugation with DNA.[55] The QY of conjugated GQDs (GQDs 50 μM) compared to non- conjugated ones was found to be 60%. Therefore, the fluorescence characteristics of the QDs remained stable despite conjugation with DNA molecules. The decrease to 40% in QY indicates that DNA conjugation introduces some degree of quenching or alteration in the fluorescence properties of the GQDs.

Table 5 QY of nonconjugated and DNA-conjugated QDs

S. no	Sample	Relative quantum yield (%)	SEM	Sample	Relative quantum yield (%)	SEM
1.	CdTe-MPA QDs	100%	2.73	N-GQDs	100%	2.4
2.	CdTe-MPA-DNA QDs 1 μM	94%	2.64	GQDs-DNA QDs 1 μM	94.4%	3.53
3.	CdTe-MPA-DNA QDs 2 μM	86.9%	2.58	GQDs-DNA QDs 2 μM	88.9%	3.23
4.	CdTe-MPA-DNA QDs 5 μM	79.8%	2.37	GQDs-DNA QDs 5 μM	80.6%	3.61
5.	CdTe-MPA-DNA QDs 10 μM	71.4%	2.78	GQDs-DNA QDs 10 μM	72.2%	3.95
6.	CdTe-MPA-DNA QDs 25 μM	64.3%	2.97	GQDs-DNA QDs 25 μM	65.6%	3.39
7.	CdTe-MPA-DNA QDs 50 μM	58.3%	2.16	GQDs-DNA QDs 50 μM	60%	2.22

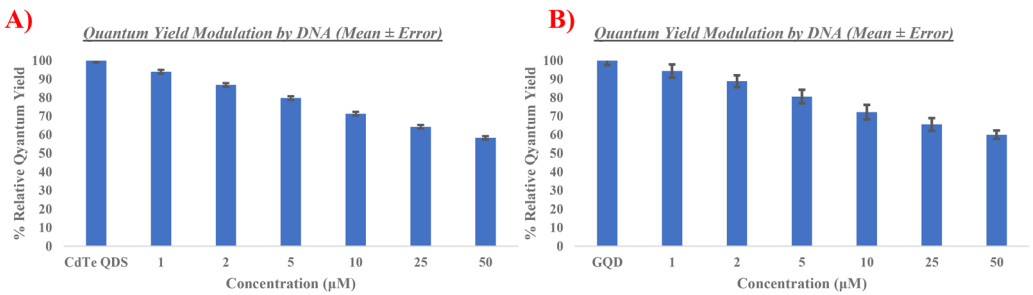

Fig. 10 (A) Plot of QY of CdTe-MPA QDs and CdTe-MPA-DNA QDs at different concentration; (B) plot of QY of GQDs and GQDs-DNA at different concentrations.

Table 6 QY of nonconjugated and cholecalciferol-conjugated QDs

S. no	Sample	Relative quantum yield (%)	SEM	Sample	Relative quantum yield (%)	SEM
1.	CdTe-MPA QDs	100%	2.19	N-GQDs	100%	2.67
2.	CdTe-MPA-cholecalciferol 1 μM	99.5%	2.4	GQDs-cholecalciferol 1 μM	99.4%	3.05
3.	CdTe-MPA-cholecalciferol 2 μM	98.8%	2.49	GQDs-cholecalciferol 2 μM	98.9%	2.46
4.	CdTe-MPA-cholecalciferol 5 μM	98.1%	2.93	GQDs-cholecalciferol 5 μM	98.3%	2.56
5.	CdTe-MPA-cholecalciferol 10 μM	97.1%	2.3	GQDs-cholecalciferol 10 μM	97.8%	3.86
6.	CdTe-MPA-cholecalciferol 25 μM	96.4%	2.29	GQDs-cholecalciferol 25 μM	97.2%	3.72
7.	CdTe-MPA-cholecalciferol 50 μM	94.8%	2.6	GQDs-cholecalciferol 50 μM	96.1%	2.63

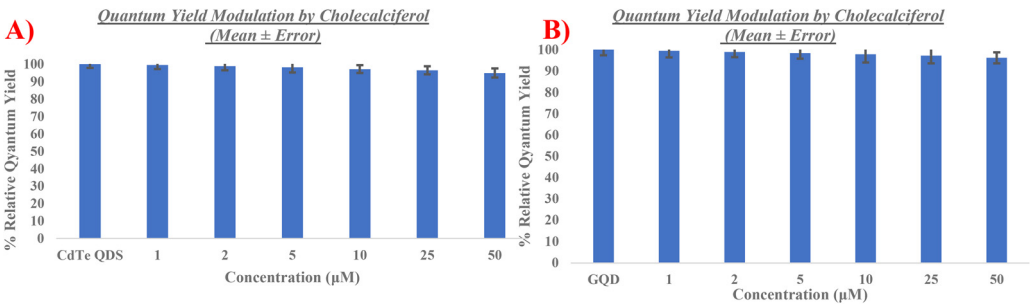

Fig. 11 (A) Plot of QY of CdTe-MPA QDs and CdTe-MPA-cholecalciferol QDs at different concentrations, (B) plot of QY of GQDs and GQDs-cholecalciferol at different concentrations.

5.7. Measurement of QY of cholecalciferol mixed QDs

Table 6 displays the QY of cholecalciferol conjugated QDs. QY at different concentrations is plotted in Fig. 11. In comparison to non-mixed CdTe-MPA QDs, the QY of mixed QDs (CdTe-MPA-cholecalciferol 50 μM) was therefore found to be 94.8%. As a result of the findings, which indicate that cholecalciferol and CdTe-MPA QDs mixture has little to no impact on the fluorescent properties of QDs, it is assumed that there is no interaction between the cholecalciferol and CdTe-MPA QDs.[56] In comparison to nonconjugated GQDs, we found that the QY of mixed QDs (N-GQDs-cholecalciferol 50 μM) is 96.1%. The findings indicate that the cholecalciferol and GQDs mixture suggests a different interaction. This lower QY indicates that, at certain concentrations, cholecalciferol may significantly affect the fluorescent properties of the GQDs.

5.8. Measurement of QY cholesterol-conjugated QDs

Table 7 displays the QY of cholesterol conjugated QDs. QY at different concentrations is plotted in Fig. 12. In comparison to non-mixed CdTe-MPA QDs, the QY of mixed QDs

Table 7 QY of nonconjugated and cholesterol-conjugated QDs

S. no.	Sample	Relative quantum yield (%)	SEM	Sample	Relative quantum yield (%)	SEM
1.	CdTe-MPA QDs	100%	2.49	N-GQDs	100%	3.9
2.	CdTe-MPA-cholesterol 1 μM	97.6%	2.46	GQDs-cholesterol 1 μM	98.9%	2.71
3.	CdTe-MPA-cholesterol 2 μM	94%	2.02	GQDs-cholesterol 2 μM	97.2%	3.19
4.	CdTe-MPA-cholesterol 5 μM	91.7%	2.73	GQDs-cholesterol 5 μM	95.6%	3.25
5.	CdTe-MPA-cholesterol 10 μM	88.1%	2.27	GQDs-cholesterol 10 μM	93.3%	3.56
6.	CdTe-MPA-cholesterol 25 μM	84.5%	3.06	GQDs-cholesterol 25 μM	91.7%	2.92
7.	CdTe-MPA-cholesterol 50 μM	81%	2.38	GQDs-cholesterol 50 μM	88.9%	2.34

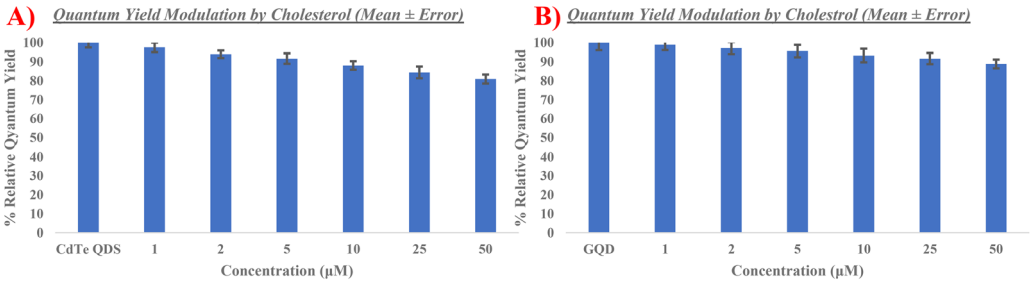

Fig. 12 (A) Plot of QY of CdTe-MPA QDs and CdTe-MPA-cholesterol QDs at different concentration, (B) plot of QY of GQDs and GQDs-cholesterol at different concentrations.

(CdTe-MPA-cholesterol 50 μM) was therefore found to be 81%. As a result of the findings, which indicate that cholesterol and CdTe-MPA QDs mixture has little to no impact on the fluorescent properties of QDs, it is assumed that there is no interaction between the cholesterol and CdTe-MPA QDs.[7] In comparison to non-mixed GQDs, we found that the QY of conjugated GQDs (GQDs-cholesterol 50 μM) is 88.9%. The findings indicate that the cholesterol and GQDs mixture suggests a different interaction. This lower QY indicates that, at certain concentrations, cholesterol may significantly affect the fluorescent properties of the GQDs.

6. Generality and broader applicability of QY modulation

The observed QY modulation is primarily governed by surface chemistry and conjugation efficiency, rather than being exclusive to CdTe or GQDs. In this study, both quantum dots possessed carboxyl (–COOH)-terminated surfaces, which enabled EDC/NHS-mediated amide bond formation with ligands containing amine ($–NH_2$) groups such as folic acid, BSA, thiamine, cobalamin, and DNA. The resultant surface modification altered the local electronic environment and radiative recombination pathways, leading to the observed QY variations. We therefore anticipate that similar ligand-dependent modulation can occur in other carboxyl-functionalized quantum dot systems, including CdSe, ZnS, CdS, carbon dots, and doped graphene dots, provided the core surface states and conjugation chemistry are comparable. In systems where the QD surface lacks reactive –COOH groups, or where the ligand does not possess complementary $–NH_2$ or reactive moieties, such modulation is expected to be minimal due to the absence of effective electronic coupling or covalent bond formation. Hence, the phenomenon is not material-specific but surface chemistry-dependent. The extent and direction of QY modulation will ultimately vary with the core composition, degree of surface passivation, and electronic nature of the conjugated ligand, all of which dictate the strength of electronic communication between the QD surface and the attached biomolecule. These insights establish a generalized framework that can be extended to other QD ligand systems, providing a predictive basis for tailoring fluorescence performance through controlled surface functionalization.[58–60]

7. Summary and conclusions

Aforementioned studies establish that QY is not a static property of quantum dots (QDs), but a highly tunable characteristic that can be precisely controlled through surface bioconjugation. By systematically examining the effects of biologically relevant ligands-including folic acid, thiamine, cobalamin, BSA, and DNA-on the PL of both CdTe-MPA QDs and nitrogen-doped graphene quantum dots (GQDs), we revealed distinct and material-dependent trends. Particularly CdTe-MPA QDs, which possess strong intrinsic fluorescence, exhibited a concentration-dependent decrease in QY after conjugation, likely due to the formation of non-radiative recombination pathways from surface-bound ligands acting as quenching sites. In contrast, GQDs, despite their initially lower QY, demonstrated remarkable fluorescence stability and, in some cases, even enhancement-particularly when conjugated with folic acid or BSA. This contrast underscores the profound influence of both the nanomaterial's core composition and the nature of the surface ligand on optical performance.

Crucially, these findings have significant implications for the field of diagnostics. The ability of GQDs to retain or even improve their fluorescence after bioconjugation makes them

especially promising for advanced imaging, biosensing, and diagnostic applications where signal stability and minimal fluorescence loss are essential. By leveraging QY modulation, researchers can design tailored nanoprobes that maximize brightness for imaging or enhance sensitivity for biosensing, thereby improving the reliability and precision of diagnostic assays. Furthermore, this approach allowed us to systematically explore and understand how the properties of the fluorophore-such as photostability, emission intensity, and environmental responsiveness-can be fine-tuned through surface chemistry. This insight is invaluable for the rational design of next-generation nanoprobes, enabling the customization of optical properties to meet specific biomedical or technological requirements. The stability of the conjugated quantum dots (QDs) was evaluated to assess their potential for biomedical applications. All ligand-conjugated CdTe-MPA and graphene quantum dots (GQDs) were stored at 0–8 °C in the dark and monitored over a period of three months. Periodic photoluminescence (PL) measurements revealed no significant change in emission intensity or spectral position, confirming that the conjugates remained optically and colloidally stable under these storage conditions. The results indicate that the prepared QD-ligand systems retained their fluorescence characteristics and structural integrity, demonstrating excellent storage stability suitable for potential bioimaging and diagnostic applications.

The ability to tune the QY through controlled bioconjugation has direct implications for molecular detection, biosensing, and fluorescence-based *in vitro* imaging. By modulating QY, fluorescence intensity and signal stability can be optimized for specific analytical and diagnostic purposes, allowing improved sensitivity and contrast in detection assays. All experiments in the present study were conducted under *in vitro* conditions only, as our focus was to establish reproducible fluorescence control through ligand conjugation. At this stage, *in vivo* studies are not planned, since such investigations would require extensive toxicological and biosafety evaluations prior to biological administration. It is also important to note that CdTe quantum dots (QDs), being heavy-metal-based, possess inherent cytotoxic potential and were therefore utilized solely for optical characterization and *in vitro* analysis. In contrast, graphene quantum dots (GQDs) offer superior biocompatibility, chemical stability, and non-toxic behavior, making them more suitable for future biological imaging and diagnostic applications. These findings highlight how controlled QY tuning can bridge the gap between nanomaterial engineering and biomedical imaging design, enabling more reliable and biocompatible fluorescence-based sensing platforms.

Overall, this work not only provides a comparative evaluation of QY modulation across different QD types and bioconjugates but also offers a practical roadmap for optimizing the balance between fluorescence and biological ligand stability. As the demand for precise, sensitive, and biocompatible nanomaterials continues to rise in medical diagnostics and related fields, the ability to control and optimize QY after functionalization will be a defining factor in the success of future nanotechnologies. By demonstrating how QY can be dynamically tuned and preserved, our study lays a strong foundation for future research into smart, responsive, and translational quantum dot-based systems, ultimately advancing the field of functional nanomaterials.

8. Placing the findings in the context of current research

The results presented here contribute to a clearer understanding of how surface chemistry influences the modulation of quantum yield (QY) in nanomaterials. Similar ligand-dependent fluorescence variations have been reported previously for semiconductor and graphene quantum dots, where the extent of surface passivation and the strength of ligand-core electronic coupling were shown to play a crucial role in governing photoluminescence behavior. In agreement with these earlier studies, the present work confirms that QY modulation is largely driven by ligand-controlled surface interactions and electronic communication between the conjugated biomolecule and the QD surface. More importantly, this study extends existing understanding by providing a reproducible experimental framework for systematically tuning fluorescence efficiency through targeted bioconjugation. These insights strengthen the broader perspective that precise control of surface chemistry offers a practical route to designing QD-based materials with predictable, stable, and optimized emission properties for sensing and imaging applications.[61–64]

Author contributions

All authors made a substantial, direct, and intellectual contribution to the paper and approved it for publication.

Conflicts of interest

The authors declare no competing financial interests.

Abbreviations

FS	Fluorescence spectroscopy
QDs	Quantum dots
CdTe-MPA	Cadmium telluride
GQDs	Graphene quantum dots

Data availability

All experimental details, synthesis procedures, and characterization data required for reproducibility have been provided in the main manuscript and the supplementary information (SI) file. The supplementary information include complete photoluminescence (PL) spectra, FTIR data, and step-by-step methodological details for each conjugate preparation. In addition, the raw spectral data supporting the findings of this study are available from the corresponding authors upon reasonable request. Together, these materials ensure full transparency

and reproducibility of the reported results. See DOI: https://doi.org/10.1039/d6ma00084c.

Acknowledgements

RPB and GS appreciate the financial support by UGC, New Delhi, India, under Faculty Recharge Program, ANRF (CRG/2022/000628), DST-UT (S&T&RE/RP/147/e-2873/(22-23)/Sanc/09/2022/905-915 Dated:-29/09/22), DHR-start up (R.12020/02/2024-HR/E-Office:8292859), ICMR (EMDR/SG/14/2023-0940), ICMR (17X(3)/*Ad-hoc*/69/2022-ITR), and ICMR (35/2/2020-Nano/BMS), DST-CSRI (DST/CSRI/2021/7), DBT (BT/PR27444/BRB/10/1645/2018), and CSIR (37/1743/23/EMR-II) Government of India. HKA acknowledges DHR, Government of India (YSS/2020/000047/PRCYSS) for the financial support. RPB and GS acknowledge the financial support from the ICMR-DHR as part of senior international fellowship.

References

1 B. Zhang, P. Zou, J. Li, D. Lu, X. J. Wang and L. Ma, *ACS Appl. Nano Mater.*, 2022, **5**, 4677–4687.
2 F. Pashley-Johnson, R. Munaweera, S. I. Hossain, S. C. Gauci, L. Delafresnaye, H. Frisch, M. L. O'Mara, F. E. Du Prez and C. Barner-Kowollik, *Nat. Commun.*, 2024, **15**, 1–9.
3 A. Banerjee, T. Pons, N. Lequeux and B. Dubertret, *Interface Focus*, 2016, **6**, 20160064.
4 B. Isherwood, P. Timpson, E. J. Mcghee, K. I. Anderson, M. Canel, A. Serrels, V. G. Brunton and N. O. Carragher, *Pharmaceutics*, 2011, **3**, 141.
5 S. V. Kilina, P. K. Tamukong and D. S. Kilin, *Acc. Chem. Res.*, 2016, **49**, 2127–2135.
6 C. Wang, X. Cui, Y. Li, H. Li, L. Huang, J. Bi, J. Luo, L. Q. Ma, W. Zhou, Y. Cao, B. Wang and F. Miao, *Sci. Rep.*, 2016, **6**, 1–8.
7 B. C. Ferrari and P. L. Bergquist, *Cytometry, Part A*, 2007, **71**, 265–271.
8 A. Bose, I. Thomas, K. G and E. Abraham, *Int. J. Adv. Pharm. Anal.*, 2018, **8**(1), 1–8.
9 R. Bose, A. Dangerfield, S. M. Rupich, T. Guo, Y. Zheng, S. Kwon, M. J. Kim, Y. N. Gartstein, A. Esteve, Y. J. Chabal and A. V. Malko, *ACS Appl. Nano Mater.*, 2018, **1**, 6782–6789.
10 H. N. Noori and A. F. Abdulameer, *Chem. Methodol.*, 2022, **6**, 842–850.
11 Z. Nguqu, O. A. Daramola and F. B. Dejene, *Results Chem.*, 2025, **15**, 102214.
12 A. Banerjee, T. Pons, N. Lequeux and B. Dubertret, *Interface Focus*, 2016, **6**, 20160064.
13 S. Tachi, H. Morita, M. Takahashi, Y. Okabayashi, T. Hosokai, T. Sugai and S. Kuwahara, *Sci. Rep.*, 2019, **9**, 1–7.
14 S. Fiedler, F. Frenzel, C. Würth, I. Tavernaro, M. Grüne, S. Schweizer, A. Engel and U. Resch-Genger, *Anal. Chem.*, 2024, **96**, 6730–6737.
15 J. Chen, Q. Zhao, B. Yu and U. Lemmer, *Adv. Opt. Mater.*, 2024, **12**, 2300873.
16 W. Q. Shi, L. Zeng, R. L. He, X. S. Han, Z. J. Guan, M. Zhou and Q. M. Wang, *Science*, 2024, **2**(383), 326–330.
17 J. Laverdant, W. D. de Marcillac, C. Barthou, V. D. Chinh, C. Schwob, L. Coolen, P. Benalloul, P. T. Nga and A. Maitre, *Materials*, 2011, **4**, 1182.
18 U. Resch-Genger, M. Grabolle, S. Cavaliere-Jaricot, R. Nitschke and T. Nann, *Nat. Methods*, 2008, **5**, 763–775.
19 N. Arumugam and J. S. Kim, *Mater. Sci. Eng. C*, 2018, **92**, 720–725.
20 K. Lawson-wood, *Fluorescene Spectrosc.*, 2018, 1–5.
21 A. Pant, T. Kaur, T. Sharma, J. Singh, A. Suttee, R. P. Barnwal, I. P. Kaur, G. Singh and B. Singh, *J. Water Health*, 2022, **20**, 1673–1687.
22 G. Singh, M. Kumar, U. Soni, V. Arora, V. Bansal, D. Gupta, M. Bhat, A. K. Dinda, S. Sapra and H. Singh, *J. Nanosci. Nanotechnol.*, 2016, **16**, 130–143.
23 M. Kumar, G. Singh, V. Arora, S. Mewar, U. Sharma, N. R. Jagannathan, S. Sapra, A. K. Dinda, S. Kharbanda and H. Singh, *Int. J. Nanomed.*, 2012, **7**, 3503–3516.
24 H. Xia, J. Hu, J. Tang, K. Xu, X. Hou and P. Wu, *Sci. Rep.*, 2016, **6**, 1–9.
25 X. Zhang, Z. Liu, L. Ma, M. Hossu and W. Chen, *Nanotechnology*, 2011, **22**, 195501.
26 N. Hildebrandt, C. M. Spillmann, W. Russ Algar, T. Pons, M. H. Stewart, E. Oh, K. Susumu, S. A. Díaz, J. B. Delehanty and I. L. Medintz, *Chem. Rev.*, 2017, **117**, 536–711.
27 D. E. Ramírez-Herrera, A. Tirado-Guízar, F. Paraguay-Delgado and G. Pina-Luis, *Microchim. Acta*, 2017, **184**, 1997–2005.
28 A. Pant, T. Kaur, T. Sharma, J. Singh, A. Suttee, R. P. Barnwal, I. P. Kaur, G. Singh and B. Singh, *J. Water Health*, 2022, **20**, 1673–1687.
29 *Cadmium Telluride Quantum Dots*, DOI: 10.1201/B16378.
30 D. Ag, R. Bongartz, L. E. Dogan, M. Seleci, J. G. Walter, D. O. Demirkol, F. Stahl, S. Ozcelik, S. Timur and T. Scheper, *Colloids Surf., B*, 2014, **114**, 96–103.
31 V. Patel, J. Shah and A. K. Gupta, *Comput. Biol. Chem.*, 2021, **93**, 107543.
32 G. Singh, M. Kumar, U. Soni, V. Arora, V. Bansal, D. Gupta, M. Bhat, A. K. Dinda, S. Sapra and H. Singh, *J. Nanosci. Nanotechnol.*, 2016, **16**, 130–143.
33 *Cadmium Telluride Quantum Dots*, DOI: 10.1201/B16378.
34 X. Yuan, Z. Liu, Z. Guo, Y. Ji, M. Jin and X. Wang, *Nanoscale Res. Lett.*, 2014, **9**, 1–9.
35 Q. Ye, L. Guo, D. Wu, B. Yang, Y. Tao, L. Deng and Y. Kong, *Anal. Chem.*, 2019, **91**, 11864–11871.
36 S. R. R. dos Reis, S. R. Pinto, F. D. de Menezes, R. Martinez-Manez, E. Ricci-Junior, L. M. R. Alencar, E. Helal-Neto, A. O. da Silva de Barros, P. C. Lisboa and R. Santos-Oliveira, *Pharm. Res.*, 2020, **37**, 1–12.
37 M. P. Romero, H. H. Buzza, M. D. Stringasci, B. M. Estevão, C. C. C. Silva, M. A. Pereira-Da-silva, N. M. Inada and V. S. Bagnato, *Int. J. Nanomed.*, 2021, **16**, 1601–1616.
38 N. T. Vo, H. D. Ngo, D. L. Vu, A. P. Duong and Q. V. Lam, *J. Nanomater.*, 2015, **2015**, 265315.
39 J. Liu, R. Li and B. Yang, *ACS Cent. Sci.*, 2020, **6**, 2179–2195.
40 J. A. Bruce and J. C. Clapper, *ACS Omega*, 2020, **5**, 26583–26591.

41 H. L. Yang, L. F. Bai, Z. R. Geng, H. Chen, L. T. Xu, Y. C. Xie, D. J. Wang, H. W. Gu and X. M. Wang, *Mater. Today Adv.*, 2023, **18**, 100376.
42 G. Singh, N. H. Zaidi, U. Soni, M. Gautam, R. Jackeray, H. Singh and S. Sapra, *J. Nanosci. Nanotechnol.*, 2011, **11**, 3834–3842.
43 J. A. Bruce and J. C. Clapper, *ACS Omega*, 2020, **5**, 26583–26591.
44 Z. A. Qureshi, H. Dabash, D. Ponnamma and M. K. G. Abbas, *Heliyon*, 2024, **10**, e31634.
45 J. Liu, R. Li and B. Yang, *ACS Cent. Sci.*, 2020, **6**, 2179.
46 J. C. Bonor, R. J. Schaefer, N. Menegazzo, K. Booksh and A. G. Nohe, *J. Nanosci. Nanotechnol.*, 2012, **12**, 2185–2191.
47 M. A. Ruiz-Robles, F. J. Solís-Pomar, G. Travieso Aguilar, M. Márquez Mijares, R. Garrido Arteaga, O. Martínez Armenteros, C. D. Gutiérrez-Lazos, E. G. Pérez-Tijerina and A. Fundora Cruz, *Nanomaterials*, 2024, **14**, 684.
48 Y. Lou, J. Ji, A. Qin, L. Liao, Z. Li, S. Chen, K. Zhang and J. Ou, *ACS Omega*, 2020, **5**, 6763–6772.
49 C. G. Sanjayan, M. S. Jyothi, M. Sakar and R. G. Balakrishna, *J. Colloid Interface Sci.*, 2021, **603**, 758–770.
50 C. S. M. Martins, A. P. Lagrow and J. A. V. Prior, *ACS Sens.*, 2022, **7**, 1269–1299.
51 N. Hildebrandt, C. M. Spillmann, W. Russ Algar, T. Pons, M. H. Stewart, E. Oh, K. Susumu, S. A. Díaz, J. B. Delehanty and I. L. Medintz, *Chem. Rev.*, 2016, **117**, 536–711.
52 M. L. Soriano, A. Jiménez-Sánchez and S. Cárdenas, *J. Sep. Sci.*, 2021, **44**, 1652–1661.
53 H. Hafian, A. Sukhanova, M. Turini, P. Chames, D. Baty, M. Pluot, J. H. M. Cohen, I. Nabiev and J. M. Millot, *Nanomedicine*, 2014, **10**, 1701–1709.
54 M. Choppadandi, A. T. Guduru, P. Gondaliya, N. Arya, K. Kalia, H. Kumar and G. Kapusetti, *Mater. Sci. Eng. C*, 2021, **129**, 112366.
55 B. C. Ferrari and P. L. Bergquist, *Cytometry, Part A*, 2007, **71**, 265–271.
56 B. C. Ferrari and P. L. Bergquist, *Cytometry, Part A*, 2007, **71**, 265–271.
57 B. Sinduja and S. A. John, *New J. Chem.*, 2019, **43**, 2111–2117.
58 U. Soni, V. Arora, G. Singh, M. Hussain and S. Sapra, *Springer Proc. Phys.*, 2013, **143**, 85–93.
59 V. L. John, Y. Nair and T. P. Vinod, *Part. Part. Syst. Charact.*, 2021, **38**, 2100170.
60 N. E. Lee, J. M. Jeong, H. S. Lim, S. Y. Lee and S. O. Cho, *Carbon*, 2020, **170**, 213–219.
61 D. A. Hines and P. V. Kamat, *J. Phys. Chem. C*, 2013, **117**, 14418–14426.
62 S. J. Lim, L. Ma, A. Schleife and A. M. Smith, *Coord. Chem. Rev.*, 2016, **320–321**, 216.
63 B. Bajorowicz, M. P. Kobylański, A. Gołąbiewska, J. Nadolna, A. Zaleska-Medynska and A. Malankowska, *Adv. Colloid Interface Sci.*, 2018, **256**, 352–372.
64 M. Yu, M. H. Saeed, S. Zhang, H. Wei, Y. Gao, C. Zou, L. Zhang and H. Yang, *Adv. Funct. Mater.*, 2022, **32**, 2109472.